Prediction of ECC tensile stress-strain curves based on modified fiber bridging relations considering fiber distribution characteristics

Bang Yeon Lee[1], Jin-Keun Kim[2] and Yun Yong Kim*[3]

[1]*University of Michigan, Ann Arbor, USA*
[2]*KAIST, Daejeon, South Korea*
[3]*Chungnam National University, Daejeon, South Korea*

Abstract. This paper presents a prediction and simulation method of tensile stress-strain curves of Engineered Cementitious Composites (ECC). For this purpose, the bridging stress and crack opening relations were obtained by the fiber bridging constitutive law which is quantitatively able to consider the fiber distribution characteristics. And then, a multi-linear model is employed for a simplification of the bridging stress and crack opening relation. In addition, to account the variability of material properties, randomly distributed properties drawn from a normal distribution with 95% confidence are assigned to each element which is determined on the basis of crack spacing. To consider the variation of crack spacing, randomly distributed crack spacing is drawn from the probability density function of fiber inclined angle calculated based on sectional image analysis. An equation for calculation of the crack spacing that takes into quantitative consideration the dimensions and fiber distribution was also derived. Subsequently, a series of simulations of ECC tensile stress-strain curves was performed. The simulation results exhibit obvious strain hardening behavior associated with multiple cracking, which correspond well with test results.

Keywords: ECC; tensile strain hardening; fiber bridging relations; fiber distribution; image analysis; variability of material properties.

1. Introduction

Micro synthetic fibers have been used to improve the toughness of quasi-brittle cement-based materials (Li *et al.* 2001, Deng and Li 2007, Roth *et al.* 2010). Especially, Engineered Cementitious Composite (ECC) is a micromechanically designed strain-hardening cementitious composite which exhibits extreme tensile strain capacity-typically more than 2%-through bridging of micro-cracks by the fibers and multiple cracking (Li and Leung 1992, Leung 1996). To predict the mechanical behavior of ECC, the fiber bridging curve and crack spacing should be precisely evaluated. Kanda *et al.* (2000) proposed a theoretical approach for predicting the tensile stress-strain relation, which is expressed in terms of steady state cracking stress, ultimate strain, and ultimate stress, of random short-fiber-reinforced cement composites showing pseudo-strain hardening. Ultimate strain is defined as the ratio between ultimate COD (crack opening displacement) and crack spacing. Ultimate stress is same to peak bridging stress in fiber bridging curve, i.e. stress-COD (crack opening displacement)

---

* Corresponding author, Professor, E-mail: yunkim@cnu.ac.kr

curve. Therefore, it is important to evaluate the fiber bridging curve and crack spacing in prediction of the uniaxial tension behavior of ECC. Fiber bridging curve and crack spacing are influenced by micromechanical parameters as well as fiber orientation (Aveston and Kelly 1973, Wu and Li 1992, Lee *et al.* 2009). However, most researchers assumed the distribution function of fiber orientation is $1/\pi$ for two dimension case or $\sin\theta$ for three dimension case.

This paper presents a prediction and simulation method for the uniaxial tension behavior of PVA-ECC that takes into consideration the fiber distribution measured by a sectional image analysis. A crack spacing equation, which quantitatively considers the fiber distribution is also derived.

2. Crack spacing

The condition for multiple cracking of a composite can be expressed by Eq. (1).

$$\sigma_{fu}V_f \geq (\sigma_{mu}V_m + \sigma_m' \, V_f = \varepsilon_{mu}E_mV_m + \varepsilon_{mu}E_fV_f) \qquad (1)$$

where σ_{fu} is the fiber strength, V_f is the fiber volume, σ_{mu} is the matrix tensile strength, V_m is the matrix volume, σ_m' is the stress on the fiber before matrix cracking, ε_{mu} is the matrix cracking strain, E_m is the elastic modulus of the matrix, and E_f is the elastic modulus of the fibers. If this condition is satisfied, the fibers that would lead matrix crack will be able to withstand additional load. Therefore, the matrix will be successively fractured into shorter lengths spacing between cracks by a process of multiple cracking, until the strain of the fiber is equivalent to the failure strain. If the failure strain of the fiber is sufficiently large, the matrix will be fractured into lengths between x' and $2x'$ where x' is determined by the rate of stress transfer between fiber and matrix. This rate of transfer is represented by the frictional strength of the interface between fiber and matrix. That is, crack spacing can be defined enough space to transfer stress from bridging fibers to matrix through interfacial friction. For continuous aligned fibers, Eq. (2) is force balance between the fiber and matrix to determine crack spacing (Aveston *et al.* 1971).

$$N\pi d_f x' \tau_0 = \sigma_{mu}V_m \qquad (2)$$

where N is the number of fibers per unit area ($= 4V_f/\pi d_f^2$), d_f is the diameter of fibers, τ_0 is frictional stress. Therefore, the crack spacing x' can be calculated by Eq. (3).

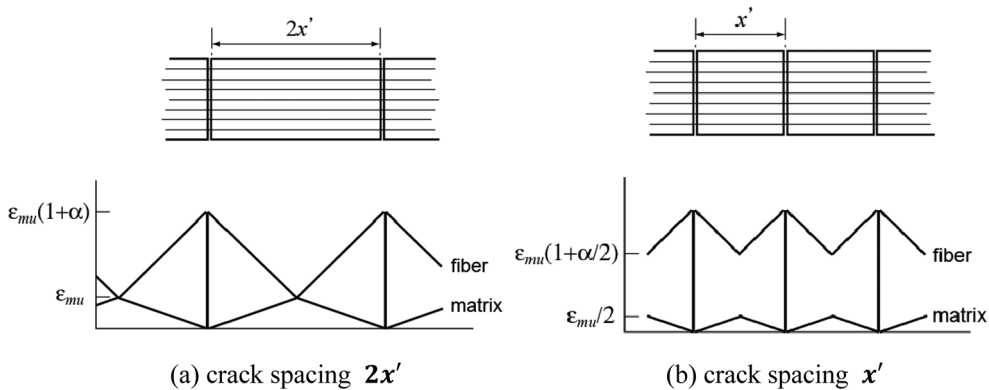(a) crack spacing **2x'**   (b) crack spacing **x'**

Fig. 1 Strain distribution after cracking of the matrix (Aveston *et al.* 1971)

$$x' = \left(\frac{V_m}{V_f}\right)\frac{\sigma_{mu}d_f}{4\tau_o} \tag{3}$$

Fig. 1 shows the strain distribution after cracking of the matrix. If the deformation of the fibers is fully elastic, the additional stress induced to the fibers will produce a maximum additional strain in the fibers of $\alpha\varepsilon_{mu}$ where $\alpha = E_mV_m/E_fV_f$. If the current crack spacing is $2x'$, the strain of the matrix at the midpoint between cracks is ε_{mu} which causes matrix cracking. Thus, the matrix fractures into lengths between the minimum crack spacing x' and the maximum crack spacing $2x'$.

2.1 Crack spacing for inclined continuous fibers

If a fiber is inclined with θ, as illustrated in Fig. 2, and the cracking spacing is x'_θ, the fiber induces a stress, $\pi d_f\tau_o x'_\theta \cos\theta$, through the interface to the matrix at a distance from the crack surface with x'_θ. At distances greater than x'_θ from the crack, the strain in the fiber and matrix will be the same. If there are $N(= 4V_f/\pi d_f^2)$ aligned fibers in a unit area of the crack surface, the number of fibers inclined with θ is $N\cos\theta$. If the probability density function of the orientation distribution of fibers is $p(\theta)$, the total number of fibers crossing the unit area of the crack surface is calculated by Eq. (4).

$$N_\theta = \int_{\theta_1}^{\theta_2} N\cos\theta p(\theta)d\theta \tag{4}$$

If the fiber orientation is randomized in two dimensions, the number of fibers per unit area is $2N/\pi$, since $p(\theta)$ is $2/\pi$. For three dimensions, the number of fibers per unit area is $N/2$, since $p(\theta)$ is $\sin\theta$.

The total stress of the matrix exerted by all fibers can be calculated by integration of the stress induced to the matrix through the interfacial friction by each fiber and the number of fibers, as expressed in Eq. (5).

$$F_{fri} = \int_{\theta_1}^{\theta_2} \pi d_f\tau_0 x'_\theta \cos\theta N\cos\theta p(\theta)d\theta \tag{5}$$
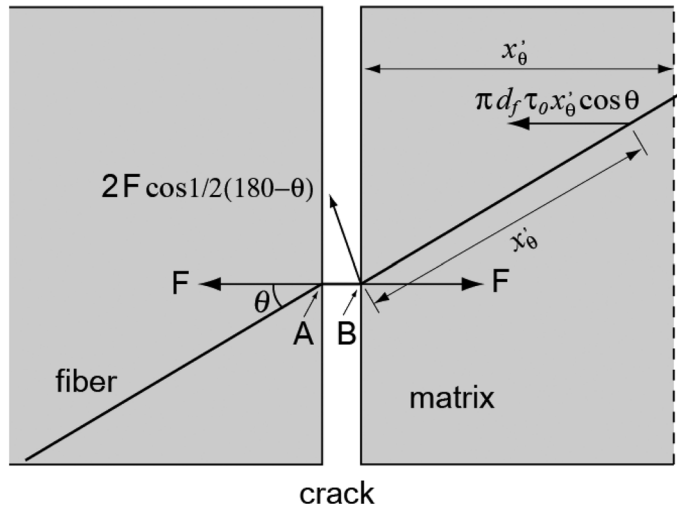

Fig. 2 Geometry assumed for a fiber crossing a crack (adopted from Aveston and Kelly 1973)

Table 1 Frictional force, pulley force, and crack spacing according to dimensions for continuous fibers

Dimension	F_{fri}	F_{pul}	x'_θ
2	$\pi d_f \tau_0 x'_\theta N \dfrac{1}{2}$	$\dfrac{\pi d_f^2}{4} \dfrac{\sigma_{mu} V_m}{V_f} N \left(1 - \dfrac{\pi}{4}\right)$	$\dfrac{\pi}{2} \dfrac{V_m}{V_f} \dfrac{\sigma_{mu} d_f}{\tau_0 4}$
3	$\pi d_f \tau_0 x'_\theta N \dfrac{1}{3}$	$\dfrac{\pi d_f^2}{4} \dfrac{\sigma_{mu} V_m}{V_f} N \dfrac{1}{3}$	$2 \dfrac{V_m}{V_f} \dfrac{\sigma_{mu} d_f}{\tau_0 4}$

Besides frictional stress, an inclined fiber exerts additional force to the matrix in the form of pulley force (Aveston and Kelly 1973). Pulley force is the reaction force of the pulley at A (Fig. 2). The force per inclined fiber is expressed by Eq. (6).

$$f_{pul} = \frac{\pi d_f^2}{4} \frac{\sigma_{mu} v_m}{V_f} 2\left(\sin \frac{\theta}{2}\right)^2 \frac{1}{\varphi_{ori}} \tag{6}$$

where φ_{ori} is the orientation coefficient ($= \int_n^{\pi/2} \cos\theta p(\theta) d\theta$). This represents the reduction rate of the number of fibers by the inclination of the fiber, and its upper bound is 1. Therefore, the total pulley force can be calculated by Eq. (7).

$$F_{pul} = \int_{\theta_1}^{\theta_2} \frac{\pi d_f^2}{4} \frac{\sigma_{mu} V_m}{V_f} 2\left(\sin \frac{\theta}{2}\right)^2 \frac{1}{\varphi_{ori}} N \cos\theta p(\theta) d\theta \tag{7}$$

The total force exerted to the matrix at a distance from the crack surface with x'_θ is then $F_{fri} + F_{pul}$. If x'_θ is the crack spacing, the following equilibrium condition is satisfied.

$$F_{fri} + F_{pul} = \sigma_{mu} V_m \tag{8}$$

From Eq. (8), x'_θ can be calculated. Table 1 presents the frictional force, pulley force, and crack spacing according to the dimensions.

2.2 Crack spacing for short random fibers

If x_d is the distance normal to the crack surface for the load in the matrix to build up to $\sigma_{mu} V_m$, the number of fibers with both ends greater than x_d from the crack surface is $N(L_f/2 - x_d)2/L_f$, since the probability density function is $2/L_f$ (Fig. 3). These fibers can fully build up σ_{mu} to the matrix and the total frictional force caused by these fibers is equivalent to that given by Eq. (9).
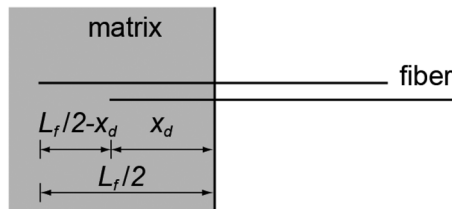

Fig. 3 Embedded length

Table 2 Frictional force, pulley force, and crack spacing according to dimensions for short random fibers

Dimension	F_{fri}	F_{pul}	x'_θ
2	$2\left(\dfrac{\tau_0 x_d V_f}{d_f} - \dfrac{\tau_0 x_d^2 V_f}{d_f L_f}\right)$	$\left(1-\dfrac{\pi}{4}\right)\sigma_{mu} V_m$	$\dfrac{L_f - \sqrt{L_f^2 - 2\pi L_f x'}}{2}$
3	$\dfrac{2}{3}\left(\dfrac{\tau_0 x_d V_f}{d_f} - \dfrac{\tau_0 x_d^2 V_f}{d_f L_f}\right)$	$\dfrac{1}{3}\sigma_{mu} V_m$	$\dfrac{L_f - \sqrt{L_f^2 - 8 L_f x'}}{2}$

$$f_{1fri} = \int_{\theta_1}^{\theta_2} \pi d_f \tau_o x_d \cos\theta N\left(1-\frac{2x_d}{L_f}\right)\cos\theta p(\theta)d\theta \tag{9}$$

On the other hand, the number of fibers having one end shorter than x_d from the crack surface is $N(2x_d/L_f)$ and their average embedded length is $x_d/2$. The total frictional force caused by these fibers is given by Eq. (10).

$$f_{2fri} = \int_{\theta_1}^{\theta_2} \pi d_f \tau_0 \frac{x_d}{2}\cos\theta N\frac{2x_d}{L_f}\cos\theta p(\theta)d\theta \tag{10}$$

Therefore, the total frictional force F_{fri} is replaced with $f_{1fri}+f_{2fri}$.

If p_1 is the load in each of n_1 fibers having both ends greater than x_d from the crack surface, the pulley force is $n_1 p_1 2(\sin\theta)^2$. Meanwhile, p_2 is the load in each of n_2 fibers having one end shorter than x_d from the crack surface, the pulley force is $n_2 p_2 2(\sin\theta)^2$. Therefore, the total pulley force can be calculated by Eq. (11).

$$F_{pul} = \int_{\theta_1}^{\theta_2} (n_1 p_1 + n_2 p_2)2\left(\sin\frac{\theta}{2}\right)^2 \cos\theta p(\theta)d\theta \tag{11}$$

For large $E_m V_m/E_f V_f$, $n_1 p_1 + n_2 p_2$ is equal to $\sigma_{mu} V_m/\varphi_{ori}$ (Aveston *et al.* 1974). Therefore, total force exerted to the matrix at a distance from the crack surface with x_d by short fibers is equal to $\sigma_{mu} V_m$. x'_θ can be calculated using Eqs. (8)-(11). Table 2 presents the frictional force, pulley force, and crack spacing according to the dimensions.

2.3 Crack spacing considering fiber distribution

If α_{nf}, which is the fiber number coefficient means the ratio of measured fiber numbers and assumed fiber numbers, is considered, Eqs. (9) and (10) can be expressed as the following equations, respectively.

$$f_{1fri} = \alpha_{nf}\int_{\theta_1}^{\theta_2} \pi d_f \tau_0 x_d \cos\theta N\left(1-\frac{2x_d}{L_f}\right)\cos\theta p(\theta)d\theta \tag{12}$$

$$f_{2fri} = \alpha_{nf}\int_{\theta_1}^{\theta_2} \pi d_f \tau_0 \frac{x_d}{2}\cos\theta N\frac{2x_d}{L_f}\cos\theta p(\theta)(d\theta)d\theta \tag{13}$$

α_{nf} can be calculated by Eq. (14)

$$\alpha_{nf} = \frac{\pi d_f^2 N_m}{4 W_f A_m \int_o^{\pi/2} \int_o^{L_f/2} p(\theta)\cos\theta dL_e d\theta} \tag{14}$$

where N_m is the number of fibers measured using image processing technique and A_m is the measured area. In Eq. (11), $n_1 p_1 + n_2 p_2$ is replaced with $\sigma_{mu} V_m / (\alpha_{nf} \varphi_{ori})$. Beyond the frictionless pulley assumption, Li *et al.* (1990) reported a snubbing effect which results in better agreement with experimental data of inclined fiber pullout tests. This can be envisioned as a flexible rope passing over a frictional pulley. In this study, the snubbing effect for crack spacing is considered as a correction factor and the correction factor is assumed to be 0.81 (Wu and Li 1992). The snubbing effect favors short crack spacing. Crack spacing that takes into quantitative consideration the dimensions, the number of fibers, and the distribution of fiber orientation can be derived using Eqs. (8), (11), and (12)-(13).

$$x_\theta' = \frac{L_f - \sqrt{L_f^2 - 4L_f \left(\frac{\varphi_{ori}\alpha_{nf} - \varphi_{Fpul}}{2} \right) \frac{\alpha_s x_1'}{\varphi_{ori}\varphi_{Ffri}\alpha_{nf}}}}{2} \tag{15}$$
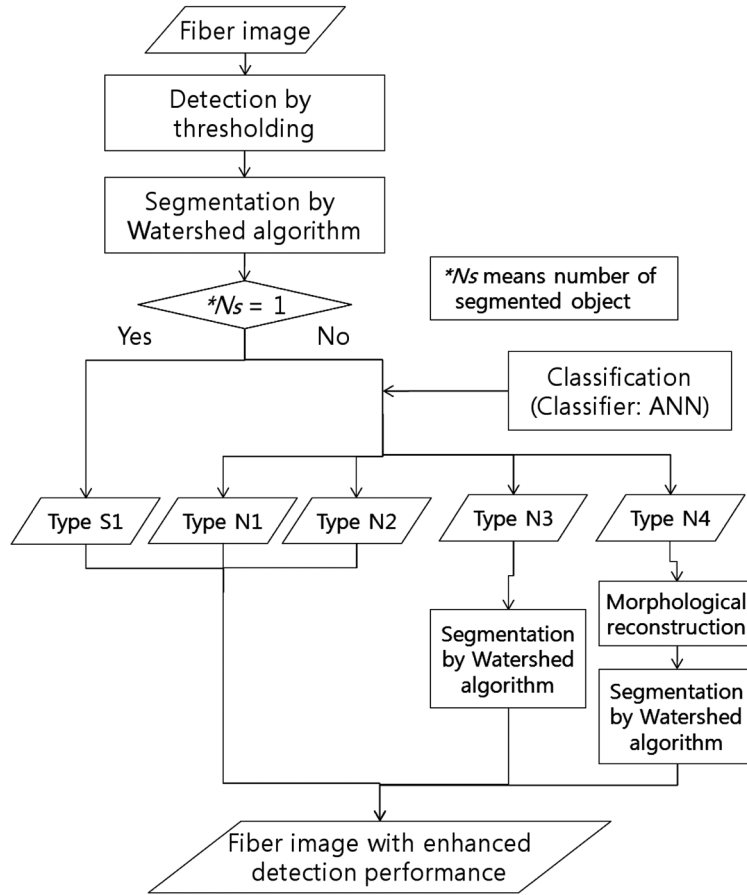
where φ_{ori}, φ_{Ffri}, and φ_{Fpul} are the orientation coefficient ($= \int_o^{\pi/2} \cos\theta p(\theta)d\theta$), the orientation coefficient for frictional force ($\int_o^{\pi/2} (\cos\theta)^2 p(\theta)d\theta$), and the orientation coefficient for pulley force ($\int_o^{\pi/2} 2\left(\sin\frac{\theta}{2}\right)^2 \cos\theta p(\theta)d\theta$), respectively. $p(\theta)$ is the probability density function for fiber orientation. α_{nf} and α_s are the fiber number coefficient and the correction factor for snubbing effect, respectively.

3. Fiber distribution evaluation

Torigoe *et al.* (2003) proposed evaluation methods for PVA fiber distribution in ECC. However, this technique has some drawbacks such as rigorous, manual fiber-counting processes and the undesirable impact of the unit size on the distribution coefficient. Lee *et al.* (2009a) proposed an automatic image processing technique to solve two drawbacks. Furthermore, the fiber detection performance was enhanced by employing the morphological reconstruction and watershed segmentation technique. The fiber distribution evaluation technique is composed of two tasks. The fiber images detected by a prototype thresholding algorithm are classified into several types by a watershed segmentation algorithm (Vincent and Soille 1991) and an artificial neural network. And then misdetected aggregate fiber images are detected correctly using the watershed segmentation algorithm and morphological reconstruction (Vincent 1993). Fig. 4 shows a flow chart of the detection algorithm. The orientation of the fiber at the cutting plane can be calculated by measuring the major axis and minor axis lengths of an object, as expressed by Eq. (16).

$$\theta = \cos^{-1}\left(\frac{l_s}{l_\varsigma}\right) \tag{16}$$

where l_s is the minor axis length and is equal to the diameter of the fiber and l_l is the major axis length of the fiber.

Fig. 4 Flow chart of enhanced detection algorithm (Lee *et al.* 2009a)

4. Numerical simulation for uniaxial tension behavior of PVA-ECC

4.1 Model of matrix and fiber bridging curve

Before the stress induced to composite reaches the cracking strength of the composite, the stress-strain relation can be expressed by the following Eq. (17).

$$\sigma_{ct} = E_c \varepsilon \quad \text{for} \quad \sigma_{ct} \leq f_{ct} \tag{17}$$

where E_c is the elastic modulus which is assumed as $E_m V_m + E_f V_f$ and f_{ct} is the first crack strength of the composite. Li and Leung (1992) derived f_{ct} in terms of the matrix toughness K_{tip} and flaw size c (Eq. 18).

$$f_{ct} = \sigma_0 g \left[\left(\frac{2\sqrt{2}}{3} \sqrt{\bar{c}} - \frac{\bar{c}}{4} \right) + \frac{\sqrt{\pi \bar{k}}}{2} \frac{\bar{k}}{\bar{c}} \right] \tag{18}$$
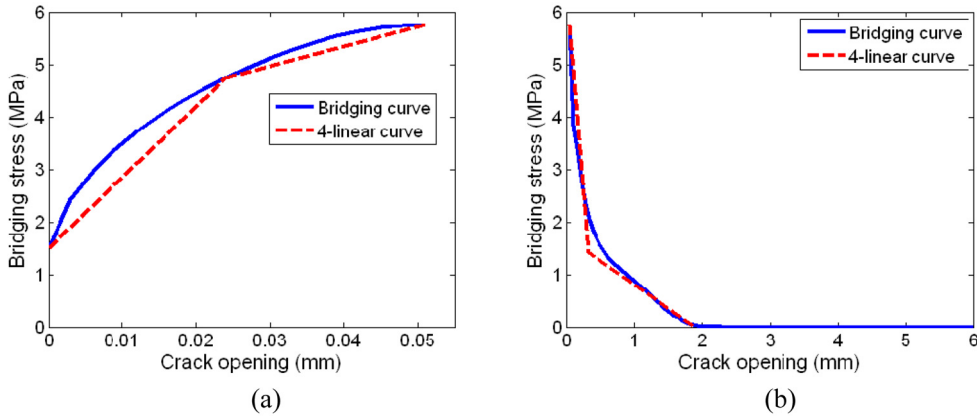
Fig. 5 Calculated and simplified bridging curve (a) prepeak, and (b) postpeak

where $\sigma_0 = \dfrac{v_f \tau_o}{2}\left(\dfrac{L_f}{d_f}\right)$, $g = \dfrac{2}{4+f^2}(1+e^{\pi f/2})$, $\hat{\delta}^* = \dfrac{2\tau_0}{E_f(1+\eta)}\dfrac{L_f}{d_f}(1+\gamma)$, $\eta = \dfrac{V_f E_f}{V_m E_m}$, $K_{tip} = K_m\left(\dfrac{E_c}{E_m}\right)$, $\overline{K} = \dfrac{K_{tip}}{\sigma_0 c_0 g \hat{\delta}^*}\dfrac{1}{}$, $c_0 = \left(\dfrac{L_f E_c}{2K_{tip}}\right)^2 \dfrac{\pi}{16(1-v^2)^2}$, $\hat{c} = \dfrac{c}{c_0}$, and $\overline{c} = \dfrac{\sqrt{c}}{\hat{\delta}^*}$

The flaw size c can be estimated by Eq. (19) (Kanda and Li 1998).

$$c = \left(\frac{\sqrt{\pi}}{2}\frac{K_m}{\sigma_{mu}}\right)^2 \tag{19}$$

where σ_{mu} is the tensile strength of the matrix and K_m is the matrix fracture toughness.

Fig. 5 shows the calculated and simplified fiber bridging curve. In this study, the fiber bridging curve was obtained using the fiber bridging constitutive law derived by Lee *et al.* (2009b) which quantitatively considers the fiber distribution. Because a fiber bridging curve considering fiber distribution can be obtained by numerical integration, a more simplified curve should be used for a simple finite element analysis. The simplified bridging curve can be a bilinear curve passing through three points, that is, the initial bridging stress, bridging stress corresponding to the half of ultimate COD and the peak bridging stress before the peak bridging stress. After peak bridging stress, the original bridging curve can be simplified by a bilinear curve whose energy is equivalent to that of the original bridging curve. To account for the variability of material properties, randomly distributed properties drawn from a normal distribution with 95% confidence ($\pm 2s$) are assigned to each element.

4.2 Analysis procedure

Under displacement controlled deformation, the composite exhibits linear elastic behavior with an elastic modulus equivalent to that of the uncracked composite. The tensile load will increase with an increase of deformation until the first crack forms at the lowest strength in the specimen. After the first crack is formed, the elastic modulus of the uncracked composite is replaced by the fiber bridging relation, i.e. the relation of the stress and crack opening. Accordingly, the load drops suddenly due to force equilibrium between the cracked section and the adjacent uncracked composite section. The load

will again increase gradually with an increase of deformation until the induced stress reaches a sufficient level to cause the formation of another crack in the composite. This process is continued until the induced stress reaches the lowest peak bridging stress (Yang and Fischer 2005).

The element size is determined on the basis of the crack spacing x'_θ described in section 3.3. A crack spacing between x'_θ and $2x'_\theta$ is expected. To consider the variation of crack spacing, the crack spacing is also randomly distributed drawn from the probability density function of $\cos\theta$.

5. Experimental verification

5.1 Material composition and properties

In this study, experimental results for a uniaxial tension test performed by Kim *et al.* (2007) are used. Table 3 and Table 4 show the mix proportions and micromechanics parameters of PVA-ECC used in this study. A polyvinylalcohol (PVA) fiber (Kuraray Co. Ltd., REC 15, Japan) was used as the reinforcing fiber with a 2% volume fraction.

Table 3 Mix proportions (Kim *et al.* 2007)

Test variables	Cement	Water	Sand	Slag	HRW[a]	HPMC[b]	V_f (%)
wc60wos	1.0	0.60	0.8	0	0	0.001	
wc60ws	1.0	0.60	0.8	0.25	0	0.001	2
wc48wos	1.0	0.48	0.8	0.25	0.02	0	
wc48ws	1.0	0.48	0.8	0	0.02	0	

[a]High-range water-reducing admixture
[b]Hydroxypropylmethyl-cellulose
All numbers are mass ratios of cement weight except fiber contents (volume fraction)

Table 4 Micromechanics parameters

	Micromechanics parameters	wc60wos	wc60ws	wc48wos	wc48ws
Fiber	Fiber length (mm)		12		
	Fiber diameter (mm)		0.040*		
	Fiber elastic modulus (GPa)		40		
	Nominal fiber strength (MPa)		1600*		
	Fiber volume fraction (%)		2		
Matrix	Crack tip toughness (MPa·m$^{0.5}$)	0.1	0.12	0.146	0.168
	Elastic modulus (GPa)	17.2	18.4	21.6	26.2
	Splitting tensile strength (MPa)	3.07	3.54	4.24	4.70
	First crack strength (MPa)	3.41	3.92	4.69	5.20
Interface	Frictional bond strength (MPa)	1.62	1.65	1.82	1.85
	Chemical bond strength (J/m^2)	1.82	1.88	1.85	1.83
	Slip-hardening coefficient	0.0582	0.104	-0.054	0.129
	Snubbing coefficient		0.30		
	Fiber strength reduction factor		0.3		

5.2 Fiber distribution

Table 5 shows the fiber distribution characteristics. ECC specimens with slag have higher fiber dispersion coefficients, which mean that ECC with slag has more uniform fiber dispersion. When the fibers are more homogeneously distributed, the fiber bridging capacity may be larger, finally leading to a larger tensile strain capacity. On the other hand, there is no correlation between F_n values and the existence of slag particles. Fig. 6 shows the probability density function for the fiber

Table 5 Fiber distribution

	Fiber dispersion coefficient	F_n (number/mm^2)		
		Measured	2D	3D
wc60wos	0.311 (0.0118)	8.95 (0.391)		
wc60ws	0.321 (0.00836)	9.94 (0.291)	10.7	8.37
wc48wos	0.315 (0.00550)	10.6 (0.968)		
wc48ws	0.317 (0.000106)	9.91 (0.144)		

All data are average values of four specimens and the numerical values in parentheses present the standard deviation
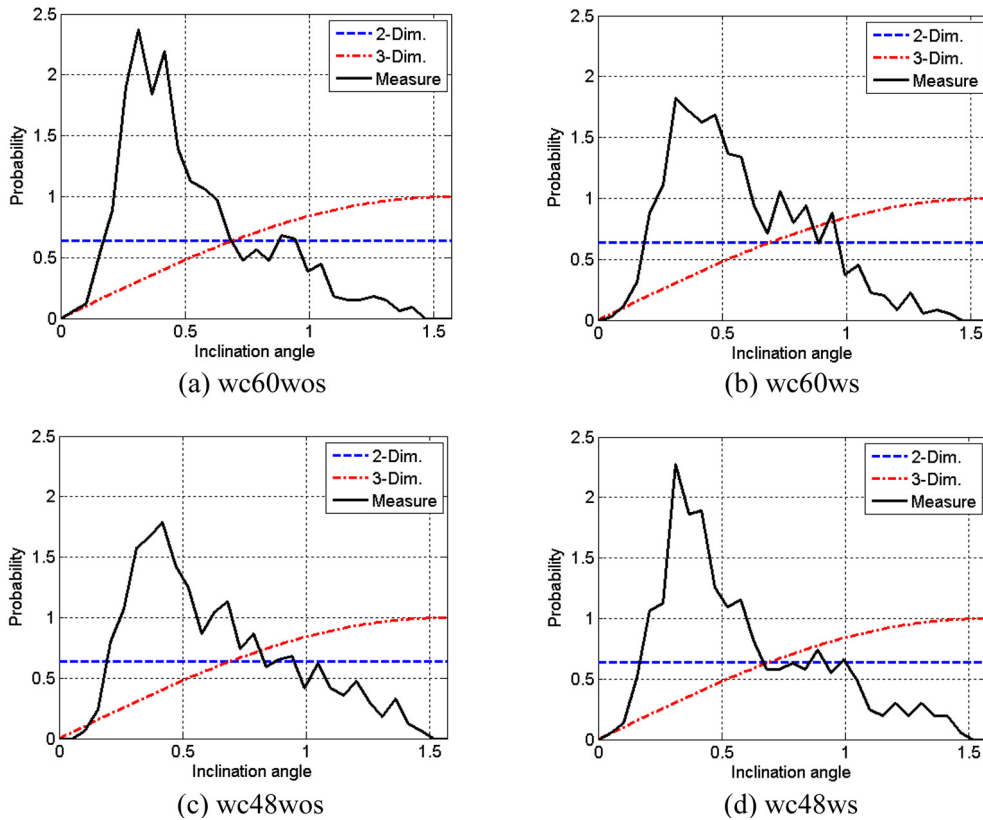

Fig. 6 Probability density functions according to mix proportions

distribution according to the specimens. The probability density functions measured by the image analysis are much different from those obtained by assuming two- or three-dimensional random distributions for the fiber distribution.

5.3 Comparison between simulation and experimental results

Fig. 7 and Table 6 show the fiber bridging curves according to the fiber distribution and specimens with different mix proportions. Table 7 presents the calculated crack spacing considering the fiber distribution. It is seen that the crack spacing increases with an increase of the strength of the matrix. Calculated crack spacing was used to simulate uniaxial tension behavior. Fig. 8 presents a comparison between simulation and experiment results of uniaxial tension behavior. The simulation results on the basis of the fiber distribution measured using an image analysis exhibit multiple cracking and strain hardening behavior similar with the test results. Although there is approximately 0.7 MPa error in the case of the wc60wos specimen, it can be seen that the predicted first crack strengths agree well with the test results. The simulation results of the wc60wos and wc48wos specimens show higher ultimate tensile strain capacity than the test results. On the other hand, the
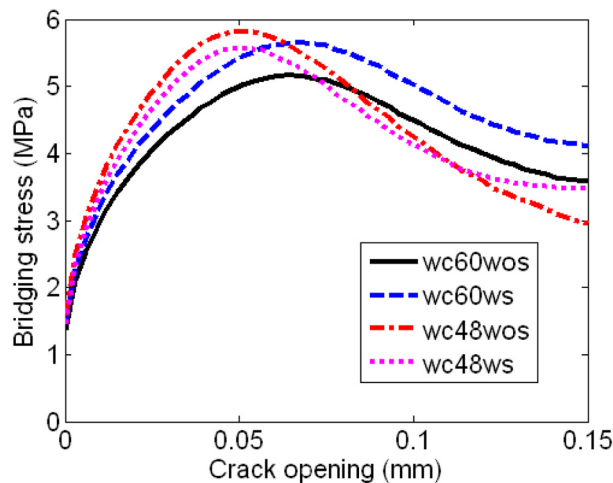

Fig. 7 Fiber bridging curve according to the fiber distribution for four specimens

Table 6 Fiber bridging characteristic according to the fiber distribution

PDF	Initial stress (MPa)			Peak bridging stress (MPa)			Crack opening displacement at peak bridging stress (μm)		
	Measured	2D	3D	Measured	2D	3D	Measured	2D	3D
wc60wos	1.33 (0.0572)	1.59	1.26	4.74 (0.256)	5.22	4	60.0 (4.24)	45	36
wc60ws	1.50 (0.0528)	1.61	1.25	5.62 (0.248)	5.28	4	64.3 (3.21)	45	36
wc48wos	1.58 (0.148)	1.59	1.24	5.85 (0.313)	5.35	4.04	52.5 (3.00)	39	30
wc48ws	1.49 (0.0198)	1.58	1.23	5.63 (0.101)	5.43	4.04	49.0 (3.46)	42	33

Measured data are average values of four specimens and the numerical values in parentheses present the standard deviation

Table 7 Crack spacing

PDF	Measured	2D*	3D*
wc60wos	1.39 (0.0528)	1.34	1.65
wc60ws	1.47 (0.0348)	1.55	1.91
wc48wos	1.54 (0.133)	1.7	2.12
wc48ws	1.81 (0.0395)	1.9	2.38

*Wu and Li 1992
All data are average values of four specimens and the numerical values in parentheses present the standard deviation

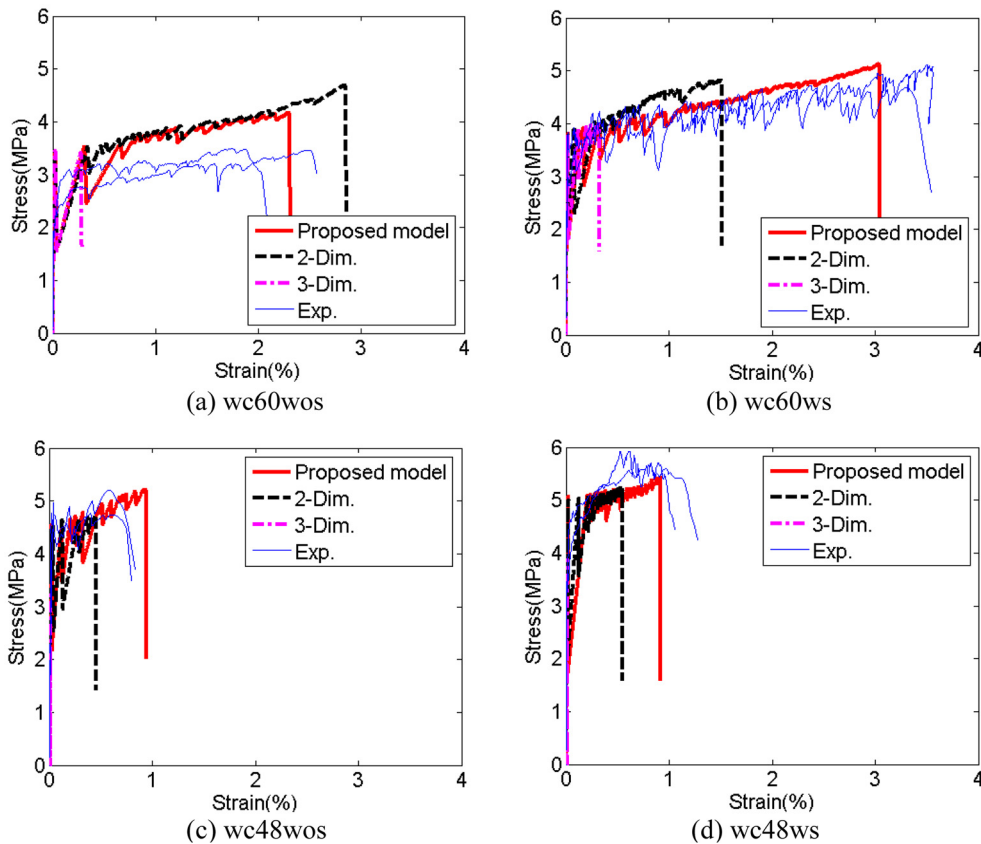(a) wc60wos   (b) wc60ws

(c) wc48wos   (d) wc48ws

Fig. 8 Comparison between simulation and experimental results of uniaxial tension behavior

simulation results of wc60ws and wc48ws show lower ultimate tensile strain capacity than the test results. These results can be explained by the variation in the fiber dispersion. Kim *et al.* (2007) found that adding slag to the matrix improves the fiber dispersion, and thus the plug pullout phenomenon can be decreased. The quantitative effect of the fiber dispersion on the fiber bridging curve is beyond the scope of this study. On the other hand, the ultimate tensile strain predicted on the basis of fiber bridging curves obtained by assuming two- or three-dimensional random distributions for the fibers exhibit about 50% and 10% of those of experimental results, respectively.

In the case of the wc60wos, the ultimate tensile strain predicted on the basis of fiber bridging curves obtained by assuming two-dimensional random distributions for the fibers exhibit about 20% higher than those of experimental results. Therefore, the present results show that the uniaxial tension behavior can be approximately predicted using the proposed method based on an image analysis of the distribution characteristics of the fibers.

6. Conclusions

This paper presents a prediction and simulation method for the uniaxial tension behavior of PVA-ECC that takes into consideration the fiber distribution measured by a sectional image analysis. A fiber distribution analysis was carried out, and the simulation results for uniaxial tension behavior were compared with the test results. The simulation results exhibit multiple cracking and strain hardening behavior similar to the test results. Although there is approximately 0.7 MPa error in the case of the wc60wos specimen, it can be seen that the predictions of the first crack strengths agree well with the test results. The simulation results of the wc60wos and wc48wos specimens show higher ultimate tensile strain capacity than the test results. On the other hand, the simulation results of wc60ws and wc48ws show lower ultimate tensile strain capacity than the test results. These results can be explained by the variation in the fiber dispersion. Adding slag to the matrix improves the fiber dispersion, and thus the plug pullout phenomenon can be decreased. From the present results, it is shown that the uniaxial tension behavior can be approximately predicted using the proposed method based on an image analysis of the distribution characteristics of the fibers.

Ackonwledgements

References

Aveston, J., Cooper, G.A. and Kelly, A. (1971), "Single and multiple fracture", In the Properties of Fiber Composites, Guildford, UK: IPC Science and Technology Press, P. 15-26.
Aveston, J. and Kelly, A. (1973), "Theory of multiple fracture of fibrous composites", *J. Mater. Sci.*, **8**, 352-362.
Aveston, J., Mercer, R.A. and Sillwood, J.M. (1974), "Fiber reinforced cements-scientific foundations for specifications, in composites-standards", Testing and Design, Proceedings of National Physical Laboratory Conference, UK, p. 93-103.
Deng, Z. and Li, J. (2007), "Tension and impact behaviors of new type fiber reinforced concrete", *Comput. Concrete*, **4**(1), 19-32.
Kanda, T. and Li, V.C. (1998), "Multiple cracking sequence and saturation in fiber reinforced cementitious composites", *Concrete Res. Technol.*, **9**(2), 1-15.
Kanda, T., Lin, Z. and Li, V.C. (2000), "Tensile stress-strain modeling of pseudo strain-hardening cementitious composites", *J. Mater. Civil Eng. - ASCE*, **12**(2), 147-156.
Kim, J.S., Kim, J.K., Ha, G.J. and Kim, Y.Y. (2007), "Tensile and fiber dispersion performance of ECC (Engineered Cementitious Composite) produced with slag particles", *Cement Concrete Res.*, **37**(7), 1096-1105.

Lee, B.Y., Kim, J.K., Kim, J.S., and Kim, Y.Y. (2009a), "Quantitative evaluation technique of PVA (Polyvinyl Alcohol) fiber dispersion in engineered cementitious composites," *Cement Concrete Comp.,* **31**(6), 408-417.

Lee, B.Y. Kim, Y.Y. and Kim, J.K. (2009b), "Fiber bridging characteristic of PVA-ECC evaluated based on the sectional image analysis", *Proceedings of ICCES'09*, Phuket, Thailand, 642-647.

Leung, C.K.Y. (1996), "Design criteria for pseudoductile fiber-reinforced composites", *J. Eng. Mech. - ASCE*, **122**(1), 10-14.

Li, V.C. and Leung, K.Y. (1992), "Steady-state and multiple cracking of short random fiber composites", *J. Eng. Mech. - ASCE*, **118**(11), 2246-2264.

Li, V.C., Wang, Y. and Backer, S. (1990), "Effect of inclining angle, bundling, and surface treatment on synthetic fiber pull-out from a cement matrix", Compos., **21**(2), 132-140.

Li, V.C., Wang, S. and Wu C. (2001), "Tensile strain-hardening behavior of polyvinyl alcohol engineered cementitious composite (PVA-ECC)", *ACI Mater. J.,* **98**(6), 483-92.

Li, V.C., Wu, C., Wang, S., Ogawa, A. and Saito, T. (2002), "Interface tailoring for strain-hardening polyvinyl alcohol-engineered cementitious composite (PVA-ECC)", *ACI Mater. J.*, **99**(5), 463-472.

Roth, M.J., Slawson, T.R. and Flores, O.G. (2010), "Flexural and tensile properties of a glass fiber-reinforced ultra-high-strength concrete: an experimental, micromechanical and numerical study", *Comput. Concrete*, **7**(2), 169-190.

Torigoe, S., Horikoshi, T. and Ogawa, A. (2003), "Study on evaluation method for PVA fiber distribution in engineered cementitious composite", *J. Adv. Concrete Technol.*, **1**(3), 265-268.

Vincent, L. (1993), "Morphological grayscale reconstruction in image analysis: applications and efficient algorithms", *IEEE T. Image Process.*, **2**(2), 176-201.

Vincent, L. and Soille, P. (1991), "Watesheds in digital spaces: an efficient algorithm based on immersion simulations", *IEEE T. Pattern Anal.*, **13**(6), 583-598.

Wu, C. (2001), "Micromechanical tailoring of PVA-ECC for structural application", Ph. D. Thesis, University of Michigan, 2001.

Wu, H.C. and Li, V.C. (1992), "Snubbing and bundling effects on multiple crack spacing of discontinuous random fiber-reinforced brittle matrix composites", *J. Am. Ceram. Soc.*, **75**(12), 3487-3489.

Yang, E.H., Wang, S., Yang, Y. and Li, V.C. (2008), "Fiber-bridging constitutive law of engineered cementitious composites", *J. Adv. Concrete Tech.*, **6**(1), 181-193.

Yang, J. and Fischer, G. (2005), "Investigation of the fiber bridging stress-crack opening relationship of fiber reinforced cementitious composites", *International RILEM Workshop on High Performance Fiber Reinforced Cementitious Composites (HPFRCC) in Structural Applications*, Honolulu, Hawai'I, 23-26 May.

CC